Probing Local Electronic Transitions in Organic Semiconductors through Energy-Loss Spectrum Imaging in the Transmission Electron Microscope

*Changhe Guo, Frances I. Allen, Youngmin Lee, Thinh P. Le, Chengyu Song, Jim Ciston, Andrew M. Minor, and Enrique D. Gomez**

Improving the performance of organic electronic devices depends on exploiting the complex nanostructures formed in the active layer. Current imaging methods based on transmission electron microscopy provide limited chemical sensitivity, and thus the application to materials with compositionally similar phases or complicated multicomponent systems is challenging. Here, it is demonstrated that monochromated transmission electron microscopes can generate contrast in organic thin films based on differences in the valence electronic structure at energy losses below 10 eV. In this energy range, electronic fingerprints corresponding to interband excitations in organic semiconductors can be utilized to generate significant spectral contrast between phases. Based on differences in chemical bonding of organic materials, high-contrast images are thus obtained revealing the phase separation in polymer/fullerene mixtures. By applying principal component analysis to the spectroscopic image series, further details about phase compositions and local electronic transitions in the active layer of organic semiconductor mixtures can be explored.

1. Introduction

Imaging of soft materials by transmission electron microscopy (TEM) remains a challenge due to the low contrast between domains and sensitivity to the electron beam. Contrast and sensitivity to radiation damage are interrelated, as the latter limits the number of electrons used for imaging. The contrast C between domains must exceed the noise in the image formation process by the minimum acceptable signal-to-noise ratio (SN). Taking the stochastic noise to be the square root of the total number of electrons that pass through a picture element, the noise is $1/\sqrt{d^2 D_c}$ for the maximum dose D_c the sample can handle and a picture element area d^2 such that d is the smallest resolvable feature size. Thus, the product $C \times d$ must be greater than $SN/\sqrt{D_c}$.[1,2] Enhancing the contrast between domains or phases continues to be a central challenge in electron microscopy of soft materials.

Contrast in the TEM between organic phases can be generated from differences in mass density,[2–4] inner potential,[5,6] diffraction,[7] elemental composition,[8] and plasmon resonances.[9–11] Mass, phase, and diffraction contrast have been critical in elucidating the structure of proteins,[12] biological assemblies,[13] block copolymers and polymer blends,[4,6,14] and many other soft materials. Spectroscopic imaging through energy-filtered TEM (EFTEM) can generate contrast between organic domains or phases using inelastically scattered electrons. For example, energy-filtered imaging at core-loss ionization edges (typically 100–1000 eV) characteristic of the constituent atoms of an organic material can map different phases based on different elemental compositions. Thus, faced with minimal mass contrast in bright-field imaging mode, core-loss elemental mapping has been applied to reveal the morphological evolution in mixtures of poly(3-hexylthiophene-2,5-diyl) (P3HT) and [6.6]-phenyl-C_{61}-butyric acid methyl ester (PCBM).[15] The large differences in sulfur and carbon densities between the components results in high-contrast elemental maps that clearly show the formation of P3HT fibers and structure coarsening during thermal annealing processes. Similarly, volume-plasmon losses (≈20–30 eV) can be used to characterize the nanostructure of P3HT/PCBM blend films based on differences in the valence electronic structure (i.e., chemistry) of each phase.[10,16,17] Unfortunately, elemental mapping using core-loss energies is only effective when significant differences in elemental composition are present, and for chemical

Dr. C. Guo, Dr. Y. Lee, T. P. Le, E. D. Gomez
Department of Chemical Engineering
The Pennsylvania State University
University Park, PA 16802, USA
E-mail: edg12@psu.edu
Dr. F. I. Allen, Dr. C. Song, Dr. J. Ciston, Prof. A. M. Minor
National Center for Electron Microscopy
The Molecular Foundry
Lawrence Berkeley National Laboratory
Berkeley, CA 94720, USA
Prof. A. M. Minor
Department of Materials Science and Engineering
University of California
Berkeley, CA 94720, USA
Prof. E. D. Gomez
Materials Research Institute
The Pennsylvania State University
University Park, PA 16802, USA

DOI: 10.1002/adfm.201502090

mapping in the volume plasmon energy-loss regime, the difficulty is that volume plasmon resonances are broad, overlap, and vary little between different organic materials. Given the rich variety of structures and functions possible through small variations in chemical structure, further approaches to generate contrast between chemically distinct phases or domains within the electron microscope are needed.

Here, we demonstrate imaging of organic semiconductor mixtures based on differences in chemical bonding probed via interband transitions at energy losses near 2 eV. Mixed systems based on organic semiconductors are important for a range of organic electronic applications, including light-emitting diodes, photovoltaics, photodetectors, and thin-film transistors.[18] Using high-resolution electron energy-loss spectroscopy (EELS) in a monochromated transmission electron microscope, characteristic interband transitions of various organic semiconductors can be identified in the electron energy-loss range close to the zero-loss (elastic scattering) peak. Significant material contrast is thus derived from spectral differences arising from different band excitations and enable chemical imaging of organic materials. Using a model system, we demonstrate the application of low-loss EFTEM imaging to characterize the phase separation in widely studied P3HT/PCBM mixtures. Through principal component analysis of the acquired EFTEM image series, we identify different phases that can be attributed to distinct material compositions.

2. Results and Discussions

EELS measurements examine the transfer of energy between the high-energy (i.e., 50–300 keV) incident electron beam and the material under study. In principle, EELS can be used to measure the available excitation energies, or electronic density of states, of semiconductors by measuring energy losses near the band gap.[11,19] Nevertheless, the energy spread of the incident electron beam, near 1 eV for field-emission sources, creates a large background that makes the extraction of the electronic absorption spectra challenging.[19] The development of monochromatic sources, which can achieve energy dispersions of ≈0.1 eV, makes the study of these electronic absorption spectra for low band gap semiconductor materials through EELS possible.

For example, we can utilize a monochromated TEM to examine the electronic absorption spectra of neat organic semiconductors as shown in **Figure 1**a. The operating voltage of the microscope was 80 kV to minimize damage by the electron beam. The small energy spread of the incident beam (full-width at half maximum of 0.1–0.15 eV) leads to clear peaks corresponding to π–π^* transitions[20] in the raw data, enabling unambiguous subtraction of the elastic background from the zero-loss peak. Modeling the background as a third-order power law in both the positive and negative energy-loss direction[19] and subtracting from the EELS data yields the spectra presented in Figure 1b, which have been normalized to the maximum peak intensity for comparison.

We can identify specific features associated with optoelectronic properties, such as the band gap of regioregular poly(3-hexylthiophene-2,5-diyl) (rr-P3HT, 1.7 eV), [6,6]-phenyl-C_{61}-butyric acid methyl ester (PCBM, 2.0 eV), and poly[(4,4′-bis(2-ethylhexyl)dithieno[3,2-*b*:2′,3′-*d*]germole)-2,6-diyl-alt-(2,1,3-benzothiadiazole)-4,7-diyl] (PGeBTBT, 1.4 eV) from the onset of the EELS intensities in Figure 1b. These absorption edges from the EELS data are consistent with the band gap energies deduced from UV–visible absorption data for organic materials discussed in Figure S1 (Supporting Information).[21] The dominant peaks in the EELS of Figure 1 can be attributed to interband transitions of the organic semiconductors, and compared to peaks measured in optical absorption experiments. For example, the peak of the π to π^* transition in P3HT occurs at around 2.6 eV, while multiple fine structures of the π to π^* absorption in PCBM are found at 3.7, 4.8, and 6.5 eV. For PGeBTBT samples, spectral transitions down to 1.7 (a small shoulder) and 1.9 eV are also identified. The EELS data are similar to the UV–visible spectra, with the exception of a blueshift in the EELS data of up to 0.25 eV (Figure S1 and Table S1, Supporting Information). Although this could partly be a result of the spectral changes caused by electron beam damage, we demonstrate below that it cannot fully explain the discrepancy between the EELS and UV–visible spectra. Other explanations for the blueshift of the EELS data include charging by the electron beam and filling of excited states from secondary X-ray radiation in the electron microscope. Nevertheless, characteristic electronic features resulting from band transitions in low energy-loss regions can be used as unique spectral signatures, and thus provide a mechanism to generate imaging contrast

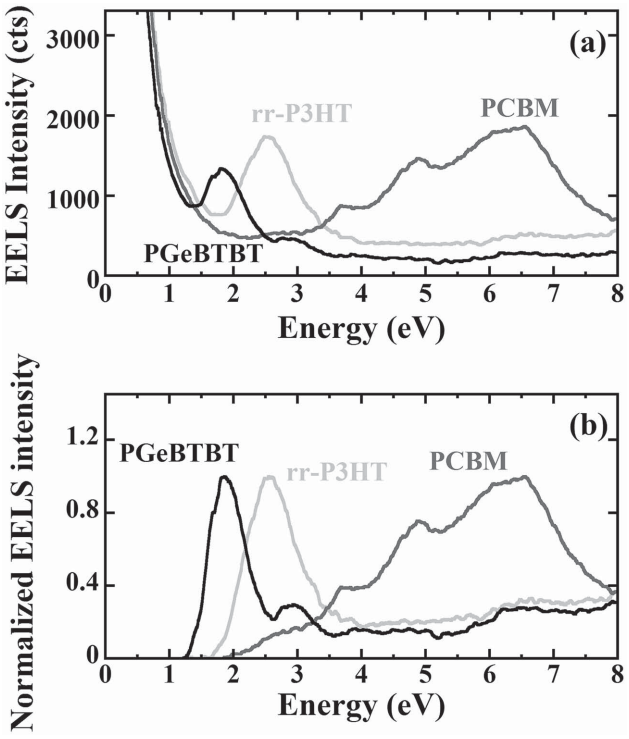

Figure 1. a) Raw EELS data and b) background-subtracted EELS data for rr-P3HT, PCBM, and PGeBTBT neat films. rr-P3HT films were annealed at 150 °C for 12 h to highlight crystalline properties. The background signal due to the zero-loss peak (<2 eV) is modeled as a third-order power law. EELS in (b) are generated by subtracting the background from the spectra in (a). EELS data are normalized by the maximum peak intensity.

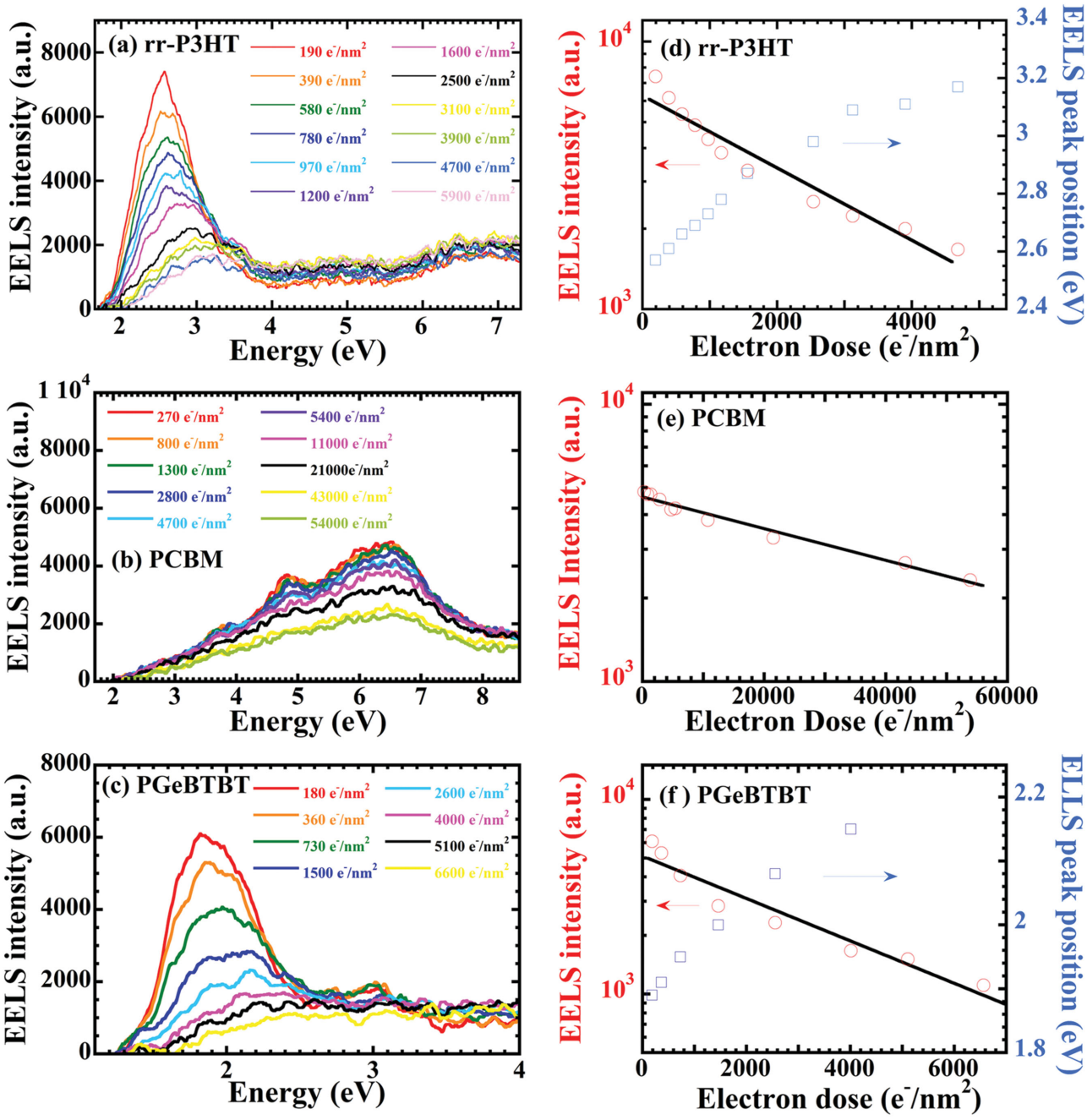

Figure 2. EELS at various radiation exposures and integrated EELS intensities in low energy-loss regions as a function of electron dose for a,d) rr-P3HT, b,e) PCBM, and c,f) PGeBTBT neat films. The solid lines represent data fits to an exponential decay. Spectral peak positions for rr-P3HT and PGeBTBT are extracted from Gaussian fits and plotted versus electron dose in (d) and (f). Intensities in (d)–(f) are presented in a log scale.

for morphological characterization in thin films of organic materials.

The electronic structure of organic materials degrades upon exposure to the electron beam, which inevitably gives rise to changes in spectral responses and contrast.[22] To investigate this, EELS measured under various exposure doses for rr-P3HT, PCBM, and PGeBTBT neat films are shown in **Figure 2**a–c, respectively. Decreases in peak intensities with increasing electron dose are observed in the electronic absorption spectra for all samples. In addition, rr-P3HT and PGeBTBT exhibit a shift in spectral peak positions toward higher energies with increasing beam damage, while the spectral features in PCBM remain at the same energies.

To quantitatively describe the effect of electron beam damage, we present the integrated intensities of the EELS peaks as a function of electron dose for three organic materials, as shown in Figure 2e,f. For rr-P3HT and PGeBTBT, the peak positions of selected peaks extracted from Gaussian fits to the EELS data

Table 1. Critical electron doses for radiation damage for various organic semiconductors estimated from EELS data.

	rr-P3HT	rra-P3HT	PCBM	PGeBTBT
Critical dose D_c [e^- nm^{-2}]	3.2×10^3	2.8×10^3	7.6×10^4	4.0×10^3

are also shown. An exponential decay in the integrated EELS intensities for the PCBM and PGeBTBT samples is observed (Figure 2e,f), while for rr-P3HT (Figure 2d), the integrated intensities initially show an exponential decay and then level off after a dose of about 4000 electron nm^{-2}. For increasing electron dose, the dominant peak in the absorption spectra of rr-P3HT gradually shifts from 2.6 eV to around 3.2 eV; the latter is similar to the position of the peak in the absorption spectra of amorphous regiorandom P3HT (rra-P3HT, see Figures S1b and S2c,d, Supporting Information). Extrapolating this absorption peak for rr-P3HT to zero electron dose yields 2.54 eV, which is 0.17 eV higher than the position of the absorption peak in optical spectra (2.37 eV, see Figure S1 and Table S1, Supporting Information). We speculate that this offset may be due to charging of the sample by the electron beam.

By fitting exponential decay curves to the integrated EELS intensities (solid lines in Figure 2d–f), the corresponding decay rate, λ, can be extracted. The maximum acceptable dose, D_c, in units of electron nm^{-2} defined as $1/\lambda$ can then be calculated, and is a measure of the sensitivity of materials to electron radiation.[14] The critical doses for rr-P3HT, regiorandom P3HT (rra-P3HT), PCBM, and PGeBTBT calculated from the degradation of low-loss spectral features can be found in **Table 1**. The critical dose from low-loss EELS for crystalline rr-P3HT is ≈3200 electrons nm^{-2}, which is an order of magnitude smaller than the critical dose determined from the decay of the diffraction peak (33 000 electrons nm^{-2}, see Figure S3, Supporting Information). Thus, the valence electronic structure is damaged prior to loss of crystallinity. PCBM is significantly more stable under irradiation than rr-P3HT with a critical dose of 76 000 electrons nm^{-2}, likely due to the stabilizing effect of the conjugated π-electron system in fullerenes and lack of C—H bonds.[22] These critical doses indicate the material radiation sensitivity and help to determine an optimum acquisition scheme to minimize the effect of beam damage for imaging experiments.

Energy-filtered TEM images from low-loss spectrum imaging of 1:1 by mass (P3HT volume fraction of ≈0.6[15] P3HT/PCBM mixtures are shown in **Figure 3**. Details on imaging conditions can be found in the Supporting Information. P3HT and PCBM have similar band gaps and similar maximum inelastic cross sections in the range of 2–10 eV,[23] but the peaks in low-loss EELS are resolved by multiple eV. Given that the spectral features from interband transitions of rr-P3HT (between 2 and 3.5 eV) degrade rapidly compared to those of PCBM (which are found between 3.5 and 8 eV), as shown in Figure 2, the EFTEM image series were acquired in the direction of increasing energy loss. In this way, the impact of beam damage on spectrum imaging is minimized. These radiation damage effects are investigated in more details below. EFTEM slices at 3, 4, 5, and 6 eV are selected from the image data set and shown in Figure 3a–d.

The EFTEM slices at 3 and 4 eV shown in Figure 3a,b reveal elongated fibers distributed within a matrix. Some background artifacts are apparent in the images obtained at the lowest energy losses, likely due to nonisochromaticity of the energy

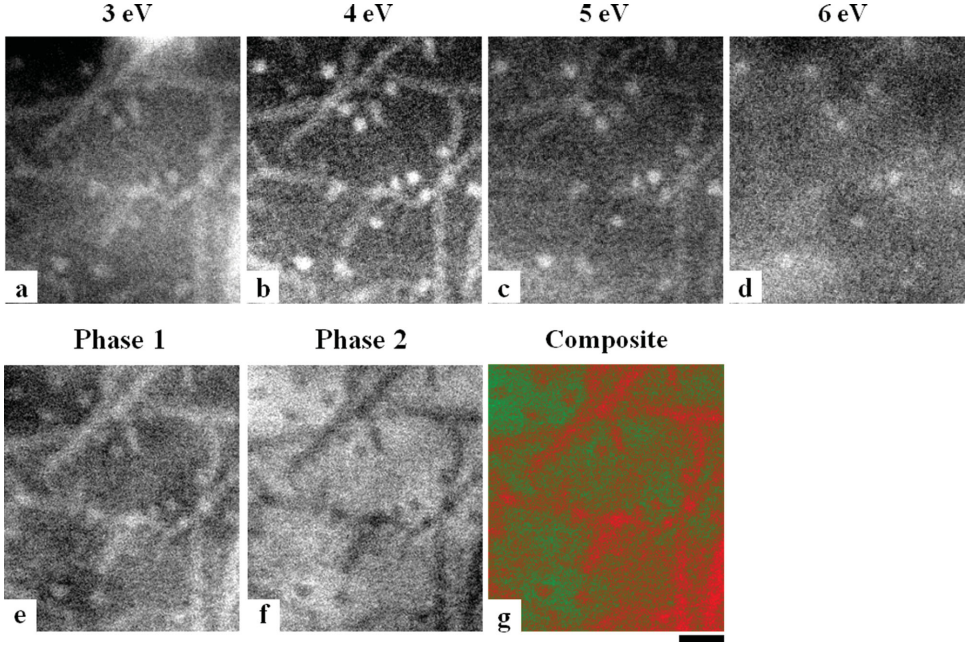

Figure 3. Low-loss EFTEM imaging of a P3HT/PCBM blend with a 1:1 weight ratio annealed at 190 °C for 30 min. a–d) EFTEM image slices taken at 3, 4, 5, and 6 eV. e,f) Phase maps deconvoluted through principal component analysis (PCA) showing spatial distributions of P3HT- and PCBM-rich domains, respectively. Image (e) highlights P3HT fibers in bright regions, while image (f) shows inverted contrast with bright areas corresponding to PCBM-rich domains. g) Composite image created by combining phase maps (e) and (f), demonstrating P3HT fibers in red and a PCBM-rich matrix in green. Scale bar is 100 nm.

filter. At 5 eV the fibrous structures are less apparent, and mostly vanish at 6 eV where PCBM exhibits strong absorption. Only fibers that are parallel to the film normal, fibers "standing up," remain visible as lighter features, suggesting more inelastic scattering at 6 eV for the fibers than the matrix. We assign the bright fibers to P3HT domains, while the dark regions correspond to PCBM (or PCBM-rich) domains.[24] This morphology is consistent with the sulfur maps shown in Figures S5–S7 (Supporting Information), and also with previously reported elemental maps.[15,25]

The phase compositions and local electronic transitions in P3HT/PCBM mixtures can be probed further through detailed analyses of the acquired low-loss spectrum images. A spectrum image dataset is effectively a 3D data cube with two spatial axes and an energy axis, because it is composed of a series of EFTEM images acquired at consecutive energy losses. Thus, for each pixel in the image an energy spectrum has been collected. A convenient method for the analysis of spectrum image datasets is the multivariate statistical technique known as principal component analysis (PCA).[16,26] PCA can differentiate the various elemental/chemical/electronic phases in the specimen as well as the random noise components in the dataset, which can then be subtracted out before further analysis is performed. Thus, PCA is a correlative technique to enhance the visibility of covarying features. PCA does not directly yield any information about the source of that covariance; it must be interpreted by other means.

After performing PCA on the low-loss spectrum image dataset for the P3HT/PCBM blend, we are able to distinguish the two polymer phases present based on differences in their low-loss spectral signatures, as shown in Figure S4 (Supporting Information). Comparing with the EELS spectra of Figure 1, where we see that P3HT exhibits stronger inelastic scattering at lower energies compared to PCBM, we assign the spectral signature extracted for the fibrous structures to P3HT-rich domains and the matrix to PCBM-rich domains as indicated in Figure S4b (Supporting Information). The energy-loss spectrum extracted for each phase can then be used for multiple linear least-squared fitting to the noise-reduced spectrum image dataset to generate chemical maps showing the distributions of P3HT- and PCBM-rich domains in the blend. These phase maps are shown in Figure 3e,f, and the composite two-phase chemical map presenting P3HT-rich domains in red and PCBM-rich domains in green is shown in Figure 3g.

The differences between the low-loss spectra extracted from the spectrum image dataset for the P3HT- and PCBM-rich domains (Figure S4, Supporting Information) are less prominent than those revealed in the EELS acquisitions of reference homopolymer samples (Figure 1). In the spectrum-imaging case, the spectral resolution is defined by the slit width selected for the acquisition (1.5 eV), whereas for the EELS acquisition the resolution is much better as defined by the monochromator settings (0.1–0.15 eV). Therefore, it is expected that the spectra extracted from the spectrum image will be more smeared out. In addition, beam damage and the presence of mixed phases will also play a role. For the EFTEM images shown in Figure 3, a cumulative dose of about 4×10^3 electron nm^{-2} was required to image up to 4 eV, while imaging up to 6 eV would have accumulated a dose over 10^4 electron nm^{-2}. Thus, while the dose is well below the critical dose for PCBM, it is close to the critical level for rr-P3HT degradation as shown in Table 1. Moreover, our previous work has indicated that the PCBM-rich matrix contains a significant amount of P3HT (in some cases up to 43% by volume).[15] Therefore the spectrum extracted for the matrix phase contains contributions from both P3HT and PCBM.

We have thus demonstrated that phase separation in P3HT/PCBM mixtures can be mapped based on differences in electronic band structures using low-loss EFTEM imaging near the band gap energies of organic materials. Previous efforts have focused on volume plasmon energy-loss imaging to characterize the morphology in polymeric thin films based on differences in the valence electron configurations of the constituent phases.[10,16] For polymer/fullerene mixtures, the bulk plasmon resonances for P3HT and PCBM have peak maxima at ≈21.5 and 25 eV, respectively, and can thus be conveniently used to generate contrast between the polymer phases by performing spectral imaging in the range of ≈18–30 eV.[23] Nevertheless, because the bulk plasmon resonances of organic materials are inherently broad, the chemical sensitivity of plasmon-loss imaging is limited, impeding the application of this technique to multicomponent systems that have similar plasmon features. In addition, elemental mapping is not applicable for systems that do not possess strong elemental contrast. Therefore, low-loss EFTEM spectrum imaging, where contrast is generated from known electronic absorptions around 2 eV, presents a much-needed alternative mapping approach.

The phase maps shown in Figure 3 are generated from excitations that occur near 2 eV. These low energy excitations should be delocalized over hundreds of nanometers, yet domains on the scale of tens of nanometers are clearly resolved in Figure 3. For organic molecules, the first excited state is a result of an electron being promoted from the highest occupied molecular orbital to the lowest unoccupied molecular orbital. The size of these excited states, or excitons, are predicted to be 1–2 nm;[27] the exciton diffusion length, which is an empirical measure of the spatial extent that excitons can explore, is near 10 nm.[28] Thus, it may be easier to spatially resolve low-loss excitations in organic molecules than in inorganic materials with delocalized valence electronic structures. Future efforts are warranted to probe the resolution limit of low-loss spectrum imaging of organic molecules.

3. Conclusions

We have demonstrated the application of EFTEM spectrum imaging at energies corresponding to interband transitions to characterize the microstructure of organic semiconductor mixtures. Electronic fingerprints resulting from band excitations reflect distinct chemical structures of organic materials, and thus provide high contrast in imaging experiments. Through optimization of the data acquisition conditions, spectral differences can be used to distinguish compositionally similar organic phases. In addition, the energy-filtered image series acquired across the low-loss spectral range enables direct extraction of local electronic states in organic films and validates the use of multivariate statistical methods for composition analysis. In this work, the applicability of this low-loss EFTEM spectrum-imaging

technique by mapping the domains within a P3HT/PCBM mixture was demonstrated, revealing P3HT fibers distributed in a PCBM-rich matrix. The imaging conditions rely on electron doses near the critical dose for damage in P3HT, but are significantly below the critical dose for PCBM. Future efforts are warranted to image at lower doses under different accelerating voltages or cryogenic temperatures to fully explore the potential of low-loss EELS. The low-loss EFTEM technique presented here is extendable to various combinations of organic materials or complicated multicomponent systems, in which differences in electronic band structures will enable mapping of the constituent components.

Supporting Information

Supporting Information is available from the Wiley Online Library or from the author.

Acknowledgements

Funding for this work was provided by NSF under Grant No. DMR-1056199. The authors thank Zhuping Fei and Martin Heeney for providing PGeBTBT. Work at the Molecular Foundry, Lawrence Berkeley National Laboratory was supported by the Office of Science, Office of Basic Energy Sciences, of the U.S. Department of Energy under Contract No. DE-AC02-05CH11231. The authors acknowledge John Asbury at Penn State for the use of a UV–vis spectrophotometer.

Received: May 21, 2015
Revised: July 30, 2015
Published online: September 2, 2015

[1] a) R. M. Glaeser, *J. Ultrastruct. Res.* **1971**, *36*, 466; b) D. C. Martin, J. H. Chen, J. Y. Yang, L. F. Drummy, C. Kubel, *J. Polym. Sci. B. Polym. Phys.* **2005**, *43*, 1749.
[2] E. L. Thomas, in *The Structure of Crystalline Polymers*, (Ed:I. H. Hall), Applied Science, London, UK **1984**, pp. 79–124.
[3] a) X. C. Chen, D. T. Wong, S. Yakovlev, K. M. Beers, K. H. Downing, N. P. Balsara, *Nano Lett.* **2014**, *14*, 4058; b) S. Yakovlev, N. P. Balsara, K. H. Downing, *Membranes* **2013**, *3*, 424; c) M. J. Park, K. H. Downing, A. Jackson, E. D. Gomez, A. M. Minor, D. Cookson, A. Z. Weber, N. P. Balsara, *Nano Lett.* **2007**, *7*, 3547; d) T. M. Chou, P. Prayoonthong, A. Aitouchen, M. Libera, *Polymer* **2002**, *43*, 2085; e) G. Kim, M. Libera, *Macromolecules* **1998**, *31*, 2569; f) K. I. Winey, E. L. Thomas, L. J. Fetters, *Macromolecules* **1992**, *25*, 2645.
[4] a) K. I. Winey, E. L. Thomas, L. J. Fetters, *Macromolecules* **1991**, *24*, 6182; b) S. P. Gido, J. Gunther, E. L. Thomas, D. Hoffman, *Macromolecules* **1993**, *26*, 4506.
[5] T. M. Chou, M. Libera, M. Gauthier, *Polymer* **2003**, *44*, 3037.
[6] D. L. Handlin, E. L. Thomas, *Macromolecules* **1983**, *16*, 1514.
[7] a) J. M. Deitzel, J. D. Kleinmeyer, J. K. Hirvonen, N. C. B. Tan, *Polymer* **2001**, *42*, 8163; b) J. T. Chen, E. L. Thomas, C. K. Ober, G. P. Mao, *Science* **1996**, *273*, 343; c) R. Henderson, J. M. Baldwin, T. A. Ceska, F. Zemlin, E. Beckmann, K. H. Downing, *J. Mol. Biol.* **1990**, *213*, 899.
[8] a) S. Yakovlev, N. P. Balsara, K. H. Downing, *Ultramicroscopy* **2012**, *116*, 39; b) S. Yakovlev, X. Wang, P. Ercius, N. P. Balsara, K. H. Downing, *J. Am. Chem. Soc.* **2011**, *133*, 20700; c) R. D. Leapman, *J. Microsc.* **2003**, *210*, 5; d) K. Varlot, J. M. Martin, C. Quet, Y. Kihn, *Ultramicroscopy* **1997**, *68*, 123; e) E. D. Gomez, A. Panday, E. H. Feng, V. Chen, G. M. Stone, A. M. Minor, C. Kisielowski, K. H. Downing, O. Borodin, G. D. Smith, N. P. Balsara, *Nano Lett.* **2009**, *9*, 1212; f) M. A. Aronova, R. D. Leapman, *MRS Bull.* **2012**, *37*, 53.
[9] a) F. I. Allen, M. Watanabe, Z. Lee, N. P. Balsara, A. M. Minor, *Ultramicroscopy* **2011**, *111*, 239; b) S. Yakovlev, M. Libera, *Micron* **2008**, *39*, 734.
[10] L. F. Drummy, R. J. Davis, D. L. Moore, M. Durstock, R. A. Vaia, J. W. P. Hsu, *Chem. Mater.* **2010**, *23*, 907.
[11] R. F. Egerton, *Rep. Prog. Phys.* **2009**, *72*, 016502.
[12] a) Y. Levi-Kalisman, G. Falini, L. Addadi, S. Weiner, *J. Struct. Biol.* **2001**, *135*, 8; b) R. Henderson, J. M. Baldwin, T. A. Ceska, F. Zemlin, E. Beckmann, K. H. Downing, *J. Mol. Biol.* **1990**, *213*, 899; c) K. A. Taylor, R. M. Glaeser, *Science* **1974**, *186*, 1036.
[13] a) B. K. Jap, M. F. Maestre, S. B. Hayward, R. M. Glaeser, *Biophys. J.* **1983**, *43*, 81; b) K. A. Taylor, R. M. Glaeser, *J. Ultrastruct. Res.* **1976**, *55*, 448; c) H. X. Sui, K. H. Downing, *Nature* **2006**, *442*, 475.
[14] D. C. Martin, E. L. Thomas, *Polymer* **1995**, *36*, 1743.
[15] D. R. Kozub, K. Vakhshouri, L. M. Orme, C. Wang, A. Hexemer, E. D. Gomez, *Macromolecules* **2011**, *44*, 5722.
[16] A. A. Herzing, L. J. Richter, I. M. Anderson, *J. Phys. Chem. C* **2010**, *114*, 17501.
[17] K. Vakhshouri, S. V. Kesava, D. R. Kozub, E. D. Gomez, *Mater. Lett.* **2013**, *90*, 97.
[18] a) R. A. Segalman, B. McCulloch, S. Kirmayer, J. J. Urban, *Macromolecules* **2009**, *42*, 9205; b) D. K. Hwang, C. Fuentes-Hernandez, J. Kim, W. J. Potscavage, S. J. Kim, B. Kippelen, *Adv. Mater.* **2011**, *23*, 1293; c) M. M. Alam, S. A. Jenekhe, *Macromol. Rapid Commun.* **2006**, *27*, 2053; d) S. R. Forrest, *Nature* **2004**, *428*, 911; e) G. Yu, J. Hummelen, F. Wudl, A. Heeger, *Science* **1995**, *270*, 1789; f) J. R. Moore, S. Albert-Seifried, A. Rao, S. Massip, B. Watts, D. J. Morgan, R. H. Friend, C. R. McNeill, H. Sirringhaus, *Adv. Energy Mater.* **2011**, *1*, 230.
[19] M. Stoeger-Pollach, *Micron* **2008**, *39*, 1092.
[20] a) F. C. Spano, *Chem. Phys.* **2006**, *325*, 22; b) F. C. Spano, *J. Chem. Phys.* **2005**, *122*, 234701; c) O. Inganas, W. R. Salaneck, J. E. Osterholm, J. Laakso, *Synth. Met.* **1988**, *22*, 395.
[21] a) Z. L. Guan, J. B. Kim, H. Wang, C. Jaye, D. A. Fischer, Y. L. Loo, A. Kahn, *Org. Electron.* **2010**, *11*, 1779; b) Z. Fei, J. S. Kim, J. Smith, E. B. Domingo, T. D. Anthopoulos, N. Stingelin, S. E. Watkins, J.-S. Kim, M. Heeney, *J. Mater. Chem.* **2011**, *21*, 16257.
[22] a) D. T. Grubb, *J. Mater. Sci.* **1974**, *9*, 1715; b) R. F. Egerton, P. Li, M. Malac, *Micron* **2004**, *35*, 399.
[23] M. Pfannmoller, H. Flugge, G. Benner, I. Wacker, C. Sommer, M. Hanselmann, S. Schmale, H. Schmidt, F. A. Hamprecht, T. Rabe, W. Kowalsky, R. R. Schroder, *Nano Lett.* **2011**, *11*, 3099.
[24] S. S. van Bavel, E. Sourty, G. de With, J. Loos, *Nano Lett.* **2009**, *9*, 507.
[25] K. Vakhshouri, D. R. Kozub, C. Wang, A. Salleo, E. D. Gomez, *Phys. Rev. Lett.* **2012**, *108*, 026601.
[26] M. Bosman, M. Watanabe, D. T. L. Alexander, V. J. Keast, *Ultramicroscopy* **2006**, *106*, 1024.
[27] C. Wu, S. V. Malinin, S. Tretiak, V. Y. Chernyak, *Nat. Phys.* **2006**, *2*, 631.
[28] a) A. Haugeneder, M. Neges, C. Kallinger, W. Spirkl, U. Lemmer, J. Feldmann, U. Scherf, E. Harth, A. Gugel, K. Mullen, *Phys. Rev. B* **1999**, *59*, 15346; b) P. E. Shaw, A. Ruseckas, I. D. W. Samuel, *Adv. Mater.* **2008**, *20*, 3516.